AN INTEGRATED GEOPHYSICAL INVESTIGATION OF KAVASILA LOW - ENTHALPY GEOTHERMAL FIELD (NW GREECE)

Thanassoulas C.[1] Gioni G.[1] Tselentis G-A[2], Dimitriadis K.[3]

PAPER PRESENTED AT THE 49th EAEG MEETING
9-12 JUNE 1986, BELGRADE YOUGOSLAVIA

[1] Institute of Geology and Mineral Exploration, 70 Messoghion Str., Athens 115-26, Greece.
[2] Athens University , Dept. of Geophysics and Geothermy, Panepistimiopolis, Ilissia, Athens 157 01, Greece.
[3] Geotest Hellas, Liakateon 49 str.. Athens 114 76, Greece.

EUROPEAN ASSOCIATION OF EXPLORATION GEOPHYSICISTS
P.O. Box 162—2501 AN The Hague—The Netherlands

ABSTRACT

In total 88 direct current resistivity soundings augmented by a small scale gravity survey and 4 SP profiles were performed during a geothermal exploration of the Kavasila NW Greece geothermal field.

The analysis of the data provided assistance in the description of the origin and driving mechanisms of the observed thermal manifestation.

The analysis of regional gravity data revealed the presence of an intrunsion with all the known surface thermal manifestations being located around the perimeter of this body.

INTRODUCTION

At the frontiers of Albany and Greece, near the city of Konitsa (NW Greece),(Fig.1), surface manifestation of low enthalpy hydrothermal activity is well known long ago.

Hot springs (T=31°C) and hot air coming out from ground fissures (T=32°) are observed in the surrounding area extended both in Greek and Albanian territory. Hot bath complexes have been developed in both countries for local use and are in operation for many years.

In order to study in detail the origin of that low enthalpy geothermal reservoire and its potential for future use in small scalel industrial activity, geological and geophysical methods of investigation were employed.

GEOLOGICAL SETTING

The investigated area is located between the river Sarandaporos and the plain of Konitsa near the Greek - Albanian border.

It is mainly occupied by flysch and Eocene limestone formations. The flysch consists of argillaceous schists and siltstone and is folded conformably with the underlying Eocene limestones. (Fig.2).

The discontinuity between flysch and Eocene limestones cannot be easily detected and there is a several meters thick transition zone which consists of thinly bedded calcite siltstone between them.

The Eocen limestones are usually thinly to medium bedded, micro-brecciated, folded and faulted. The extensive development of karst throughout the limestone massifs is a feature of great importance. This karstification is being controlled mainly by the network of vertical joints, which appears to be more significant.

Both in the Sarandaporos river and Konitsa plain, great thickness of recent overburden occur. These material are cobbles and pebbles consisting of peridotites, gabbros, quartzites, sandstones, limestones and dolomites, while in some locations, depending on local conditions lenses of sand and silt size

material are found.

Finally, quaternary river terraces appear at the northern outcrop of Konitsa plain.

ELECTRICAL RESISTIVITY SURVEYS

In total 88 resistivity soundings were completed as part of the exploration effort. The measurements were taken in two different stages. The first stage of the survey consisting of traverses T_{1a} - T_{7a} and T_8 was completed during September - November 1985, while the second stage consisting of traverses T_{1b} - T_{5b} was completed during summer 1986, (Fig.3).

All the soundings are grouped in eight traverses with a mean distance of 200m between soundings for traverses T_1 - T_6, 1500m for traverse T_7 and 100m for traverse T_8.

Because of the high topographic relief and the high level of vegetation, current electrodes were separated along the profile lines. The maximum current electrode spacing was 1600m (AB/2=800m) for all the soundings except for a small number of soundings towards the center of the investigated area, for which a spacing of 4000m was adopted.

Spatial change of apparent resistivity

The amount of data so recorded can provide an insight into the three - dimensional distribution of geoelectric parameters in the area. Figures $4_{a,b,c}$ show the apparent resistivity contours over the area with AB/2 equal to 100, 250 and 500m.

Because of the irregular topographic relief of the investigated area, we take as reference level the horizontal central part of traverse T_1 and all measurements are adjusted to this level by employing the following formula:

$$AB/2_{cor} = AB/2_{100,250,500} + H$$

where H is the difference in altitude between the corresponding sounding and the reference level.

Judging from these diagrams we see that a) the curves follow an almost NW - SE trend. This is in agreement with the direction of contact between the flysch and the limestone which is clearly exposed northern of the city of Konitsa.

b) For all AB/2 = 100, 250, 500m the apparent resistivity becomes maximum (ρ_a>100 Ohm.m) towards the E-NE part of the area. This pattern reflects the shallow depth of the limestone formations.

c) Areas with apparent resistivitiy values less than 100 O.m correspond to considerable thicknesses of the flysch cover.

From the above graphs we can see also areas with very low apparent resistivities in a NW - SE direction, occuring within the flysch cover. These low values might be:

1) due to variations of the topographic relief. In some cases

this is confirmed by superimposing the apparent resistivity map on the topographic map. Indeed, the topography of the area might change the apparent resistivities by changing the geometric factor of the electrode arrangement.

2) due to a local differantiation of the electric properties of the flysch.

3) Finally it can be due to the circulation of hot mineralized water.

From the tectonic point of view the main fault zones encountered in the area have a NW - SE trend while a main fault zone with the same direction is located towards the eastern part of the area where the limestone is exposed. This is also clear from the apparent resistivity maps where we can observe high apparent resistivity gradients.

As far as the circulation of hot water is concerned, an important role play the faults located in the limestone bedrock which reflect areas with high hydraulic conductivity, and correspond to low resistivity values within the flysch cover.

VERTICAL VARIATION OF FORMATION RESISTIVITY

The interpretation of the apparent resistivity curves was performed in two stages. During the first stage we used 2 and 3 layer model curves; with the auxiliary point method we found an approximate geoelectric model (Mundry et al 1979). Next we used a computer program based on Ghosh's method to improve the above model until the RMS difference between observed and calculated data was less than 3%. The geoelectric model thus reflects a possible geoelectric section.

The obtained geoelectric models for traverses T_1 - T_8 are shown in Fig.5.

As seen from the obtained geoelectric sections (Fig.5), the following two formations are mainly encountered:

(1) A formation with electric resistivities greater than 120 Ohm.m and sometimes up to 2000 Ohm.m corresponding to the limestone bedrock.

(2) A formation with resistivities less than 120 Ohm.m corresponding to flysch.

In some places, and in particular towards the central part of traverse T_1 a surface formation corresponding to river deposits is encountered.

Traverse T_8.

The first geoelectric traverse that was performed was traverse T_8, and consisted of six geoelectric soundings separated by only 100m.

As the interpretation diagram (Fig.5_8), shows, the location of the hot springs lies above a fault within the limestone bedrock. Another fault within the bedrock can be easily located between sounding sites 4 and 5.

An interesting feature of the above solution is the low resistivity zone between soundings 4 and 3. This might correspond to hot mineralized water flowing from the nearby fault in the bedrock and having as a result the decrease of the formation's electrical resistivity.

Traverse T_1

Judging from the apparent resistivity graph and the corresponding geoelectric section of the above traverse (Fig.5_6), we observe the following.

a) The geoelectric bedrock comes closer to the surface between soundings 28 - 34 and -2 - -10, while dips towards the center of the traverse. As it can be seen from both the apparent resistivity and geoelectric sections, the geoelectric bedrock is characterized by a great number of faults, and portays an almost "horst type" morphology below soundings 6-8 and 18-20. The existence of the horst below sites 6-8 was confirmed by gravity measurements and corresponds to limestone formation while the second horst type structure below sites 18-20 is atributed to a local differentiation of the electrical resistivity of the flysch.

b) The flysch formations covering the area show large lateral variations in their electrical resistivity. It is characteristic to note the low resistivity values encountered above horst 18-20 of the geoelectric basement and might reflect the circulation of hot mineralized water.

c) The projection of the Kavasila hot springs on the axis of traverse T_1 coincides with the location of the fault within the bedrock below sites 26 - 28.

d) Very interesting is the low resistivity layer located between sites -7 and -2 and might be due to the circulation of hot mineralized water within the bedrock.

Traverse T_2

The obtained geoelectric and apparent resistivity sections, reveal the same tectonic features as previously. Thus, the geoelctric basement is characterized by many faults while three horsts can be located below sites 11-13, 21-23 and 0 (Fig.5_5), with a coinsiderable decrease in the electrical resistivity of the flysch formation overlying them.

By comparing the geoelectric sections T_1 and T_2 we observe a difference in the absolute depth of the limestone bedrock, indicating the existence of a fault zone between the axes of the above traverses and with the bedrock diping towards the south. The same fault zone can also be seen from the apparent resistivity graphs (Fig.4).

Traverses T_3, T_4, T_5, T_6

The derived geoelectric sectionsfor traverses T_3,T_4 shown in Fig.5 respectively. The geoelectric basement dips towards the center of the traverse and is characterized by many faults and horst type structures below sites 10, 6, -4 and 31, 23, 17 and -2.

Traverse T_5 shows a very steep dipening of the geoelectric basement towards its terminal part while three horsts can be located below sites 22, 5 and 9.

Finally traverse T_6 indicates a homogeneous nature of the flysch with a fault within the geolectric basement, located below sites 3-4.

Traverse T_7

This traverse was carried out in order to obtain a general picture of the geoelectric section within the Konitsa valley.

The limestone bedrock is located up to sounding site 3, diping gradually from left to right, by a number of faults within the limestone basement and which can be followed up in the flysch and the river deposits (Fig.5).

SELF POTENTIAL INVESTIGATIONS

Owing to their link with water flow through the electrokinetic phenomena, the natural electric potentials (SP) can in many cases pinpoint areas which can be significant geothermal targets.

In recent years, both the use of the SP method and the effort to study the mechanisms of generation of potential anomalies have increased significantly, since a strong correlation between SP anomalies and geothermal activity was discovered (e.g. Zohdy et al 1973, Rapolla 1974, Diaz 1980, Corowin and Hoover 1979).

In the following, we report the results of four SP surveys carried out along traverses T_3, T_1, T_6 and T_4 and compare them with the results obtained from the geoelectric investigations.

The measurements were performed employing a high impedance millivoltmeter. The noise problems related to electrodes have been overcome through the use of copper - copper sulfate electrodes with a large contact area, avoiding the watering of the soil and carrying out the measurements in a short time.

The adopted procedure for the measurements consisted in using a stepwise advancement by 50m of the measuring dipole (gradient method), and finally integrating the obtained results.

SP Traverses T_1, T_4, T_3

In Fig.6a we compare the measured Self Potential curve for traverse T_3 with the obtained geoelectric section. The correlation between the obtained SP anomalies and the faults in the geoelectric basement is obvious.

A characteristic SP anomaly measuring -30 mV is traced above the existing hot springs and a fault in the basement, while a

broad SP anomaly measuring -20 mV is located above sites 4-6 where the geoelectric basement is characterized by an abrupt deepening.

Another, smaller SP anomaly can be seen towards the right end of the profile and probably indicates the existence of a fault within the basement.

Fig.6$_b$, depicts the obtained SP curve along traverse T_1. An anomaly measuring -25mV is located above sites 4-8. It is important to mention that the limestone bedrock outcrops at site 0 of this traverse, while on the other hand the well known hot springs just after the Greek Albany border are projected above the location of this anomaly. It is thus logical to attribute this anomaly to the movement of hot mineralized water from a fault within the limestone bedrock.

Another two SP anomalies measuring about 10 mV can be seen above the two horsts of the basement below sites 18 and 20 while a smaller one can be traced below sites 27-29 and can be correlated with the Kavasila hot springs. The great difference in altitude between the location of the Kavasila hot springs and the measuring site where the above anomaly is observed might be a possible explanation of the small magnitude of this anomaly.

A significant anomaly can also be located between sites 31-37 and is above the exposed limestone bedrock, and might indicate the circulation of water within the limestone.

In Fig.6$_c$, we represent the obtained SP curve along traverse T_3. Judging from this figure we see that no significant variation of the SP is observed except from a small change in the slope of the measured curve above sounding site 2 which coincides with the location of a graben type structure in the basement. The insignificant amplitude of the anomalies might be attributed to the great depth of the basement.

Finally, in Fig.6$_d$, we compare the results from the SP measurements along traverse T_4 with the results obtained from the geoelectric investigations. The good correlation between the bay type SP anomaly and the horst type structure of the basement is obvious.

SPATIAL VARIATION OF THE BEDROCK

The results of the geoelectric interpretations with information about the possible depth to the bedrock are compiled in Fig.7, which shows the spatial variation of the depth to the geoelectric bedrock for the whole of the investigated area.

A reference level of +400m a.s.l is adopted with the calculated depths being positive above it and negative below it.

First feature to be noted from the above map is a NW - SE fault zone confined between isodepths 0 and 200m to the east of the investigated area, while another fault zone almost parallel to the previous one is located towards the center of the area, and is confined by isodepths -100m and -200m.

Another feature is the existence of some tectonic horsts with a

NW – SE direction. One of these is located towards the center and SE part of the investigated area with a minimum depth to the top from the reference level of the order of -100m.

Fig.8, depicts the main fault zones derived from the analysis of the geoelectric data. Judging from this figure we observe that there are mainly two sets of faults, one striking towards the NW-SE and the other striking towards the NE-SW.

GRAVITY INVESTIGATIONS

Being a superposition of gravity effects of all density contrasts in a geological structure, the gravity field offers a vast amount of information.

During the present investigation we carried out a gravity profile across traverse T_1 in order to investigate the deep structure of the area.

We used for the measurements a Lacoste – Romberg Model-G gravity meter and the measured anomaly together with the calculated theoretical for an optomized model are shown in Fig.9.

The obtained results confirm those obtained from the resistivity surveys, indicating that the valley has a grabben type structure with a considerable depth towards its center.

Finally we used the existing regional gravity data (Makris 1977), and Fig.10,depicts the obtained best fit model indicating the existence of an intrusion body which might be responsible for the geothermal activity in the area, because all the known surface manifestations are concentrated around the perimeter of this body.

CONCLUSIONS

The geoelectric investigations showed that two geoelectric formations are encountered with electrical resistivities up to 120 Ohm.m for the flysch and greater than 120 Ohm.m for the limestone.

Within the flysch there are some zones of low resistivity which can be interpreted as due to alteration zones resulting from the upward movement of thermal waters from faults within the limestone basement.

This is in agreement with the existence of hot springs at sites where significant fault zones have been located in the basement (e.g. T_3: sites 1-3, T_1: sites 26-28).

A borehole which was put down after the geophysical survey (BH2, Fig.5_a), proved to be productive and yielded water of temperature of the order of 31°C. Temperature measurements which were carried out in this borehole resulted in an almost zero temperature gradient (Fig.11_a), confirming the circulation of water, entering the borehole.

A similar borehole (BH1, Fig.5_a), which was drilled prior to the geophysical survey proved unsuccesful (Fig.11_b).

The traced SP anomalies, seem to be directly related and

interpetable in terms of the thermal water circulation system, the driving force of which might be the intrusion body located from the analysis of the regional gravity data.

REFERENCES

Corowin, R. F., and Hoover, D.B., 1979. The self potential method in geothermal exploration. Geophysics 44, 226-245.

Diaz, C.S., 1980. Self potential survey northwest of Cerro Prieto. Geothermics, 9, 27-37.

Makris, J., 1977. Geophysical investigations of the Hellenides. Ed. Hamburg University, 103pp.

Mundry, E., and Homilius, J., 1979. Three layer model curves for geoelectrical resistivity measurements. H.B.G.R.

Rapolla, A., 1974. Natural electrical field survey in three southern Italy geothermal areas. Geothermics 3,3, 118-121.

Zohdy, A.A.R., Anderson, L.A., and Muffler, L.J.P., 1973. Resistivity, self potential and induced polarization surveys of a vapor dominated geothermal system. Geophysics, 38, 6, 1130-1144.

CAPTIONS OF ILLUSTRATIONS

Fig.1: Location map of the investigated area.
Fig.2: Geological setting of the investigated area. Qt= Quaternary deposits, Q.al= alluvium, Fi,Fo= flysch, Ek= limestone.
Fig.3: Location map of the geoelectric soundings.
Fig.4: Spatial variation of apparent resistivities for defferent curent electrode separations.
Fig.5: Geoelectric profiles and proposed geoelectric models.
Fig.6: Self potential profiles.
Fig.7: Map showing the depth to bedrock.
Fig.8: Map showing the location of the main fault zones within the bedrock.
Fig.9: Gravity profile across traverse T_1 with the calculated theoretical curve and the corresponding optimized model.
Fig.10: 3D modelling of the gravity field of the investigated area. Depth to the top of the first slab = 5Km, thickness of each slab = 700m.
Fig.11: Stratigraphy, Core recovery and temperature of the two boreholes, together with the corresponding geoelectric model for BH1.

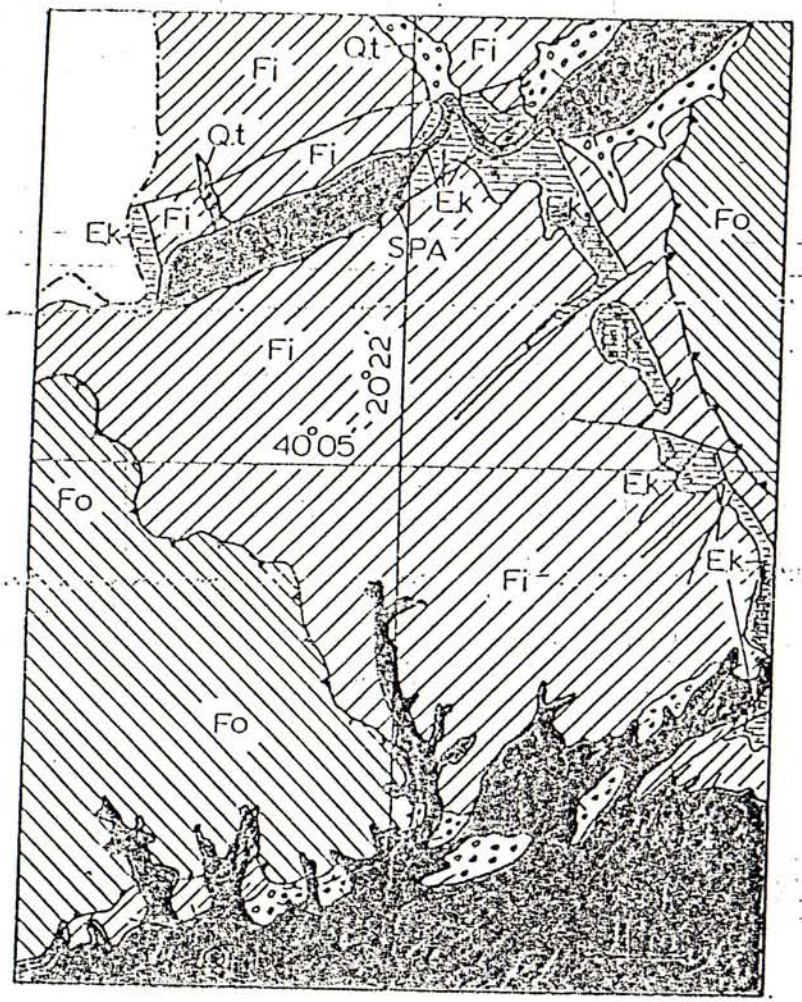
Fi
Qt
Fi
Qt
Fi
Ek
Fi
Ek
Ek
Fo
SPA
Fi
20°22
40°05
Ek
Fo
Fi
Ek
Fo

FIG. 2

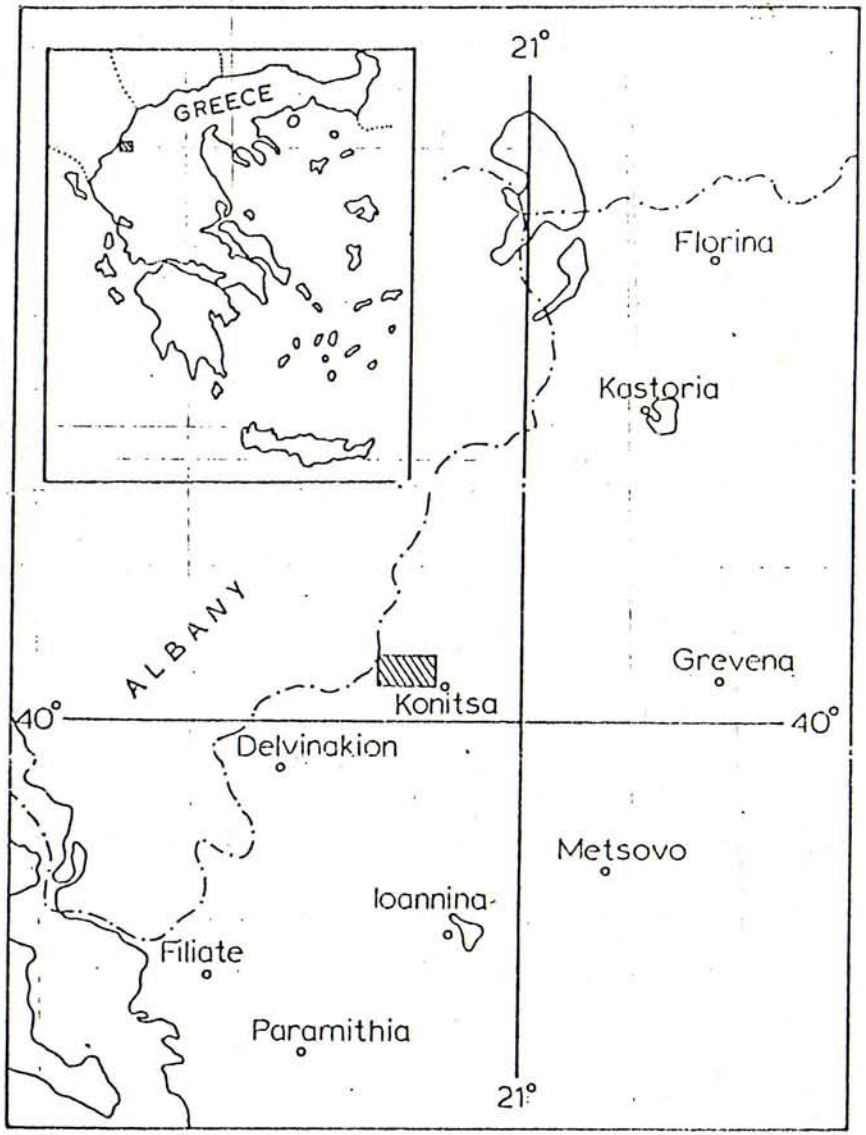
GREECE
21°
Florina
Kastoria
ALBANY
Konitsa
Grevena
40°
40°
Delvinakion
Metsovo
Ioannina
Filiate
Paramithia
21°

FIG. 1

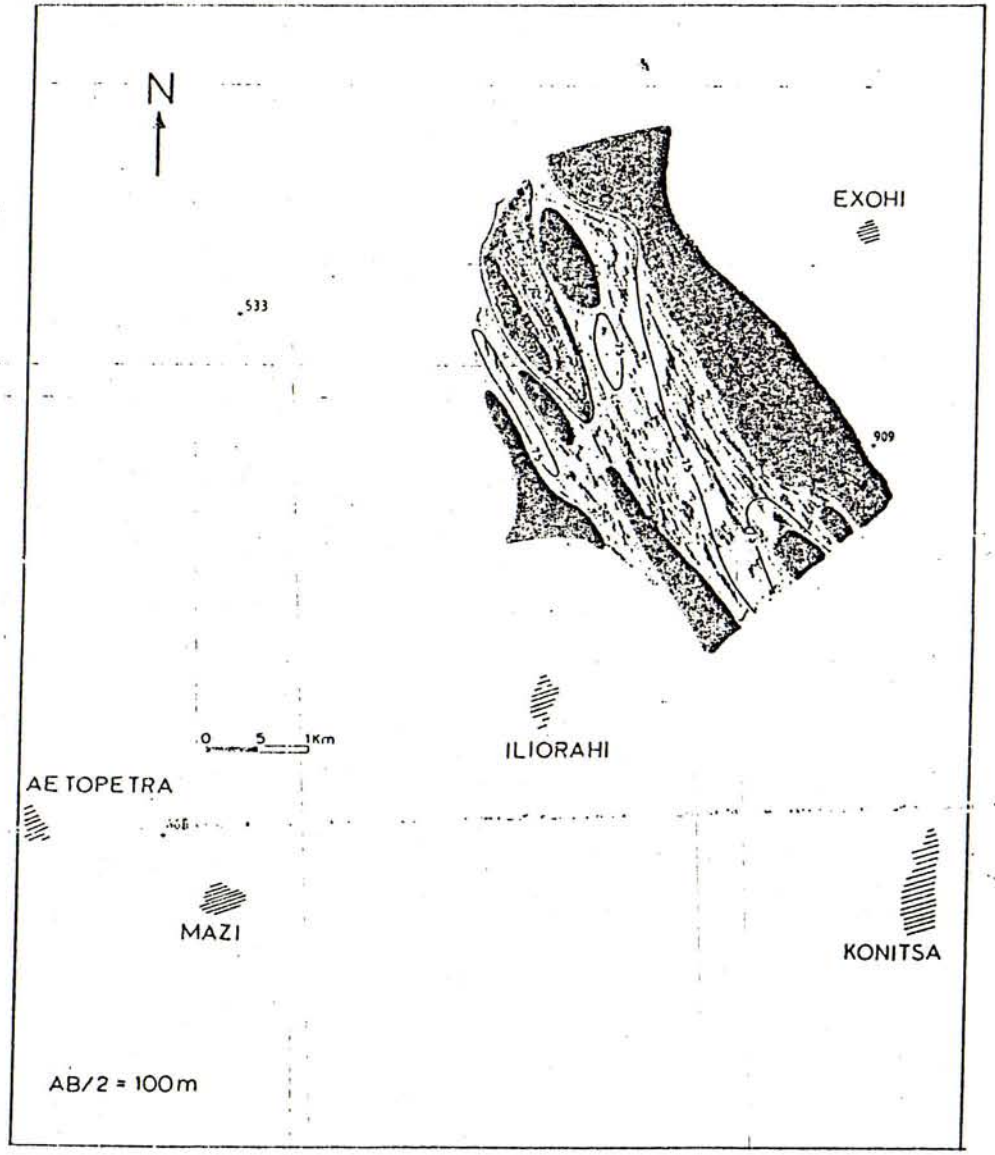
N
EXOHI
533
909
ILIORAHI
0 5 1Km
AETOPETRA
MAZI
KONITSA
AB/2 = 100m

FIG. 4a

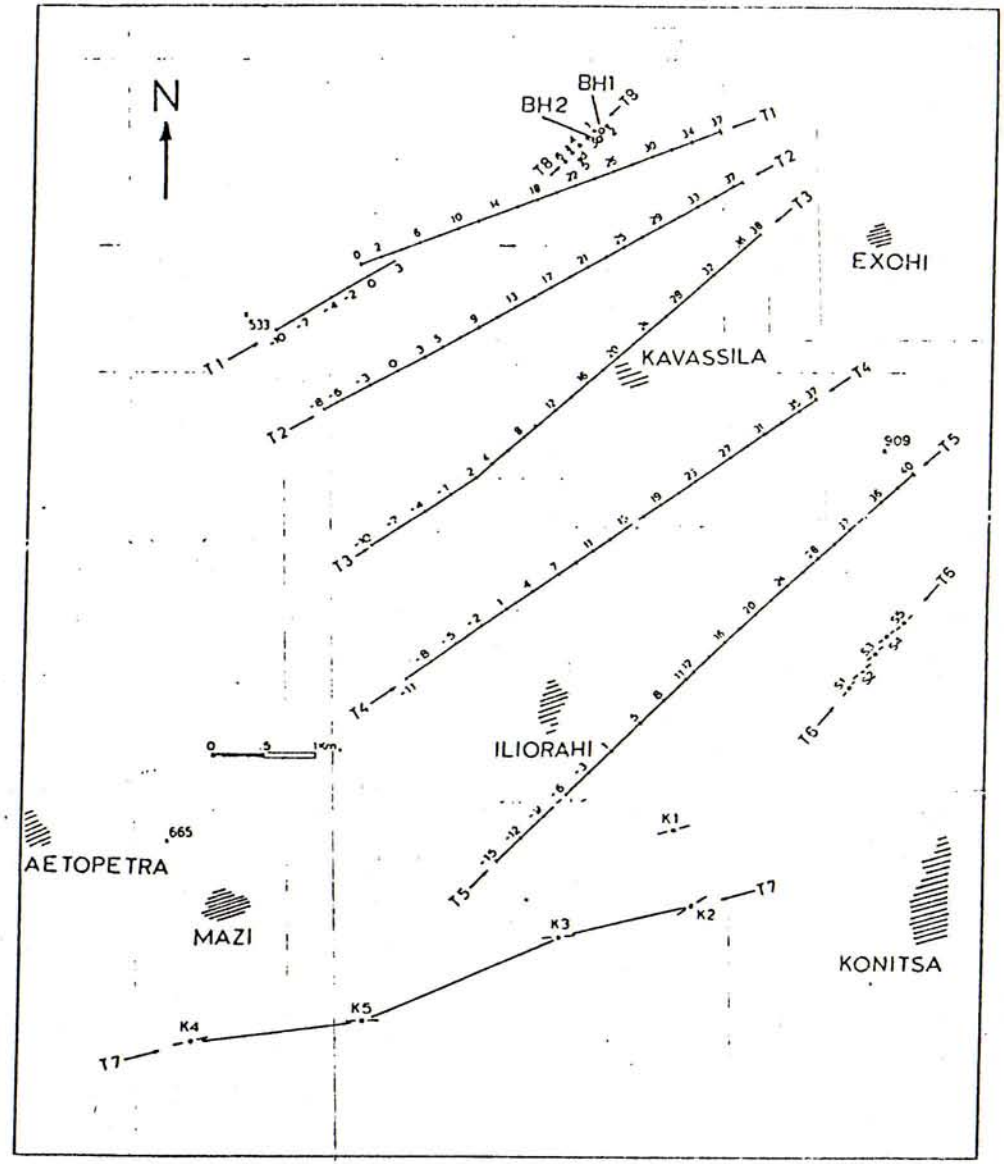
N
BH1
BH2
T8
T1
T2
T3
T4
T5
T6
T7
EXOHI
KAVASSILA
909
ILIORAHI
0 3 1Km
AETOPETRA
665
MAZI
KONITSA
K1
K2
K3
K4
K5

FIG. 3

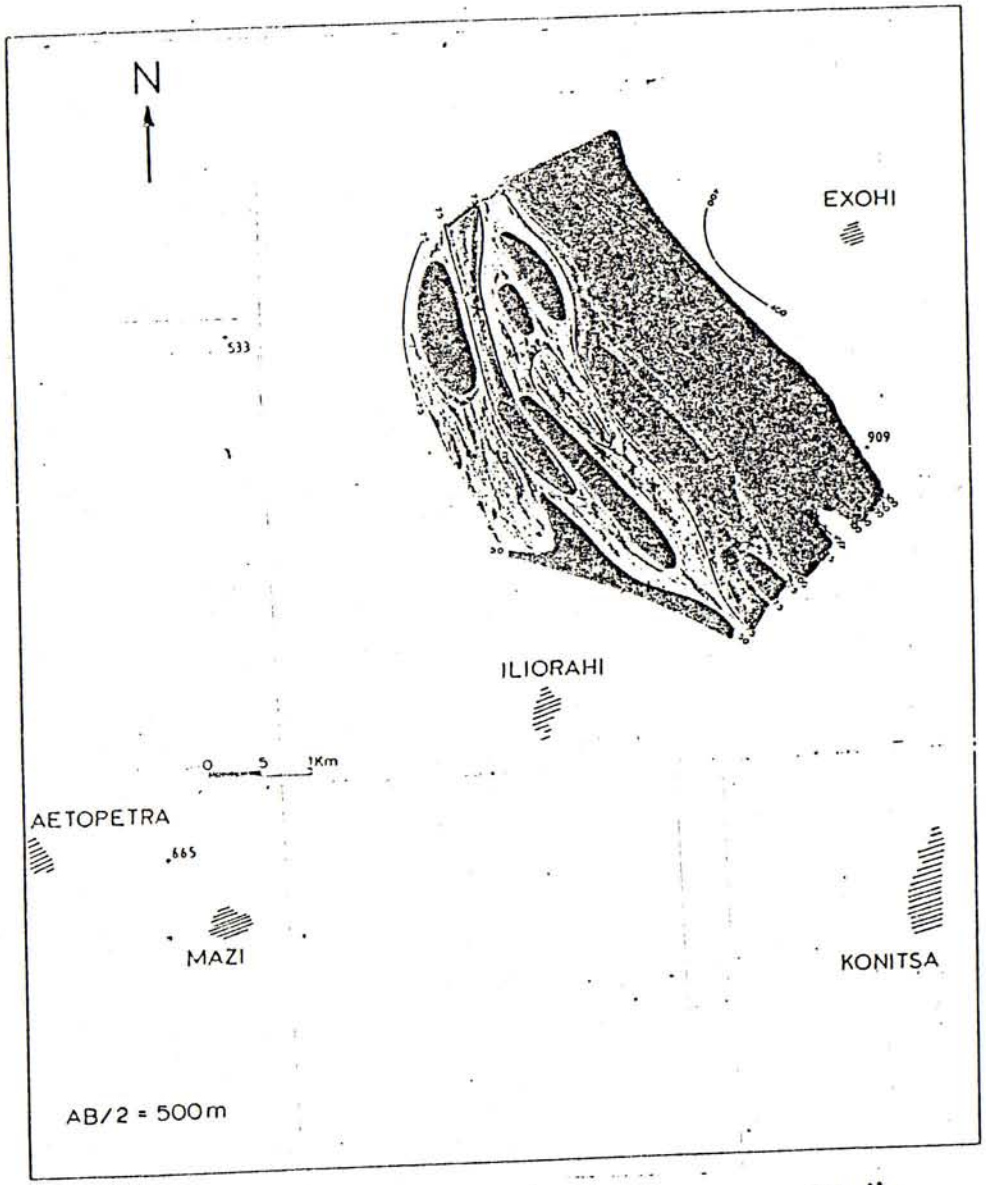
N
EXOHI
533
909
ILIORAHI
0 5 1Km
AETOPETRA
665
MAZI
KONITSA
AB/2 = 500m

FIG. 4a

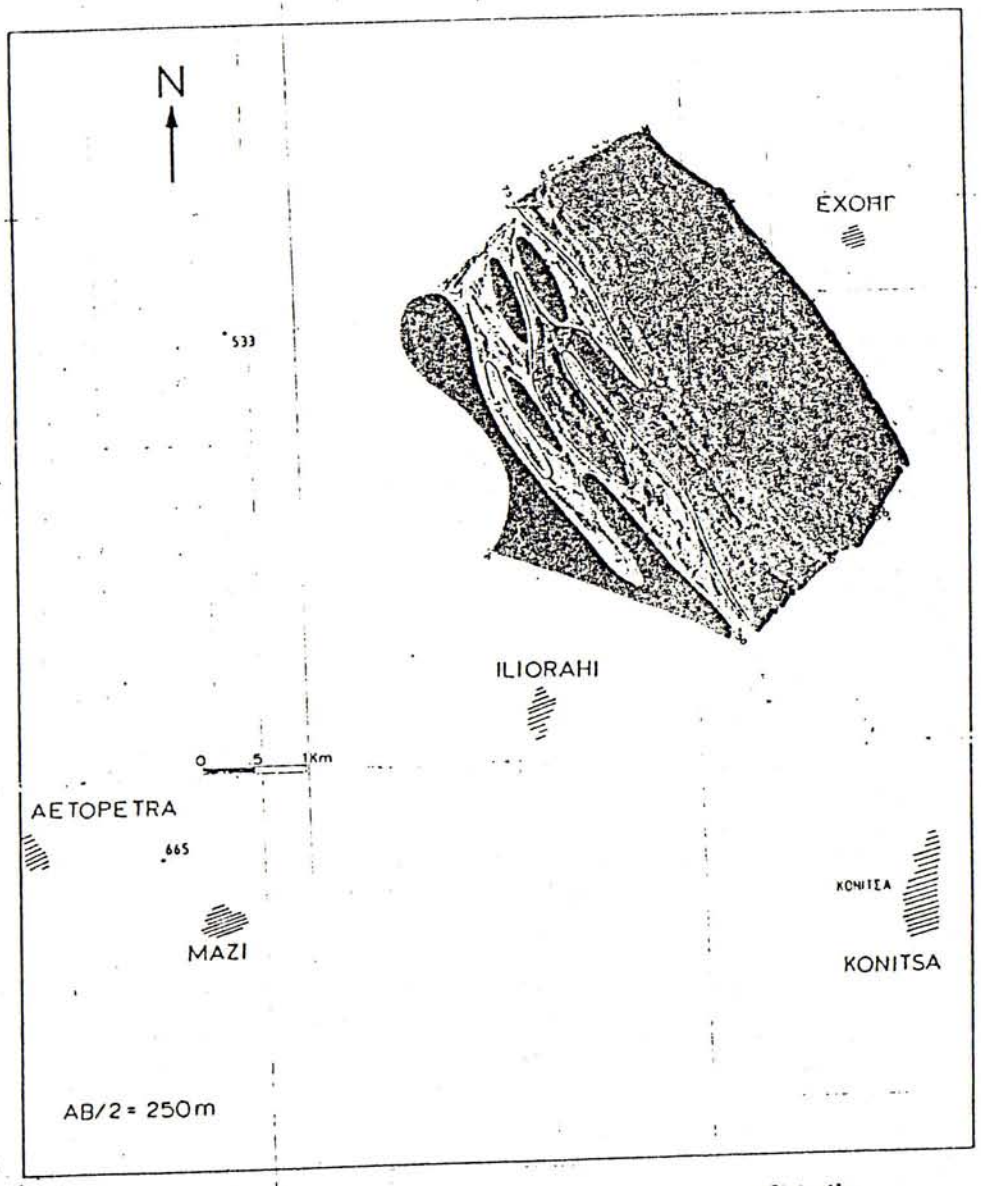
N
EXOHI
533
ILIORAHI
0 5 1Km
AETOPETRA
665
MAZI
KONITSA
AB/2 = 250m

FIG. 4b

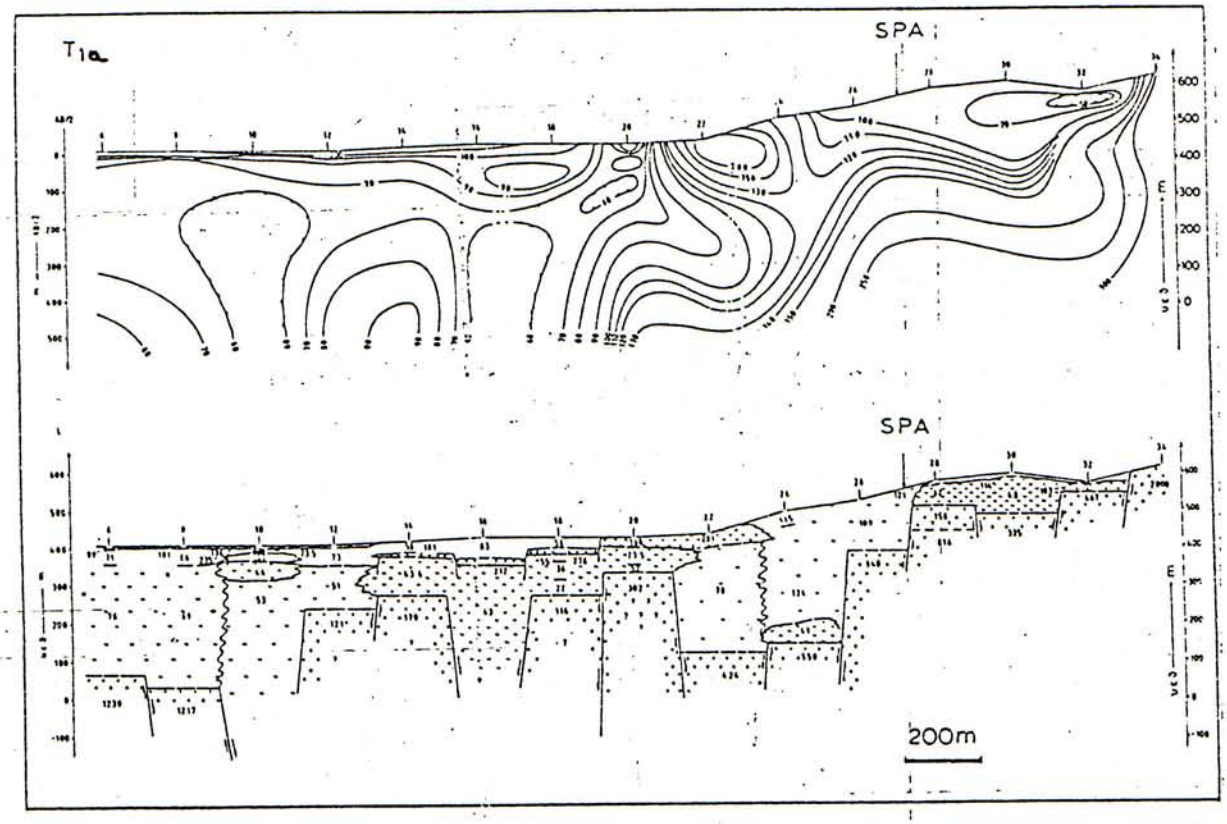

FIG 5a

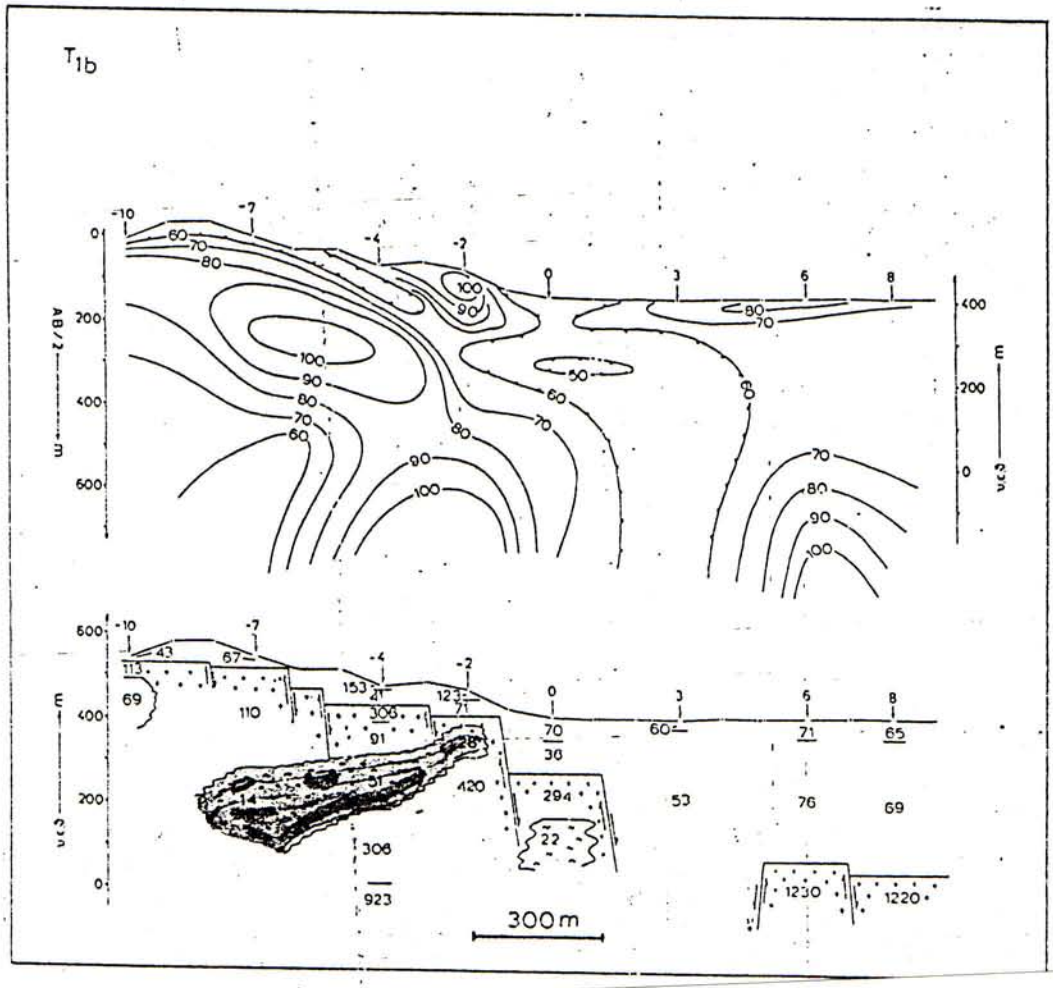

FIG. 5b

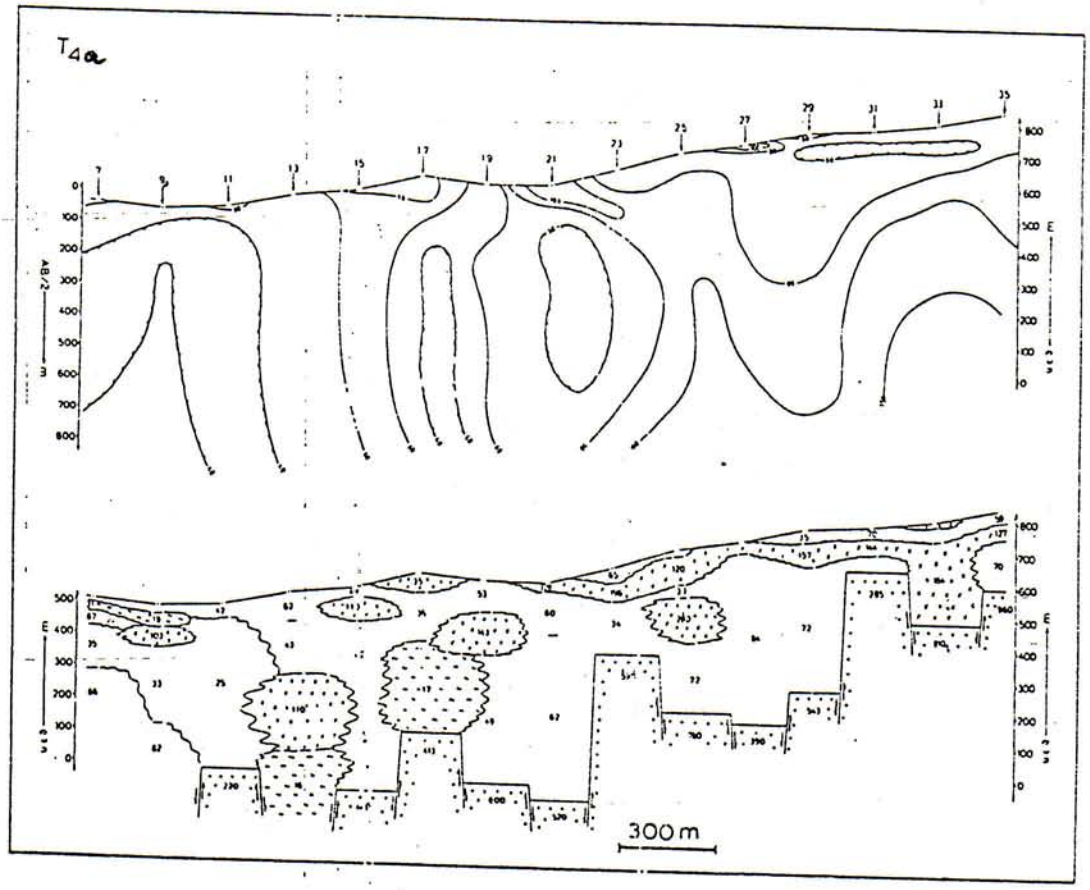

Fig. 5a

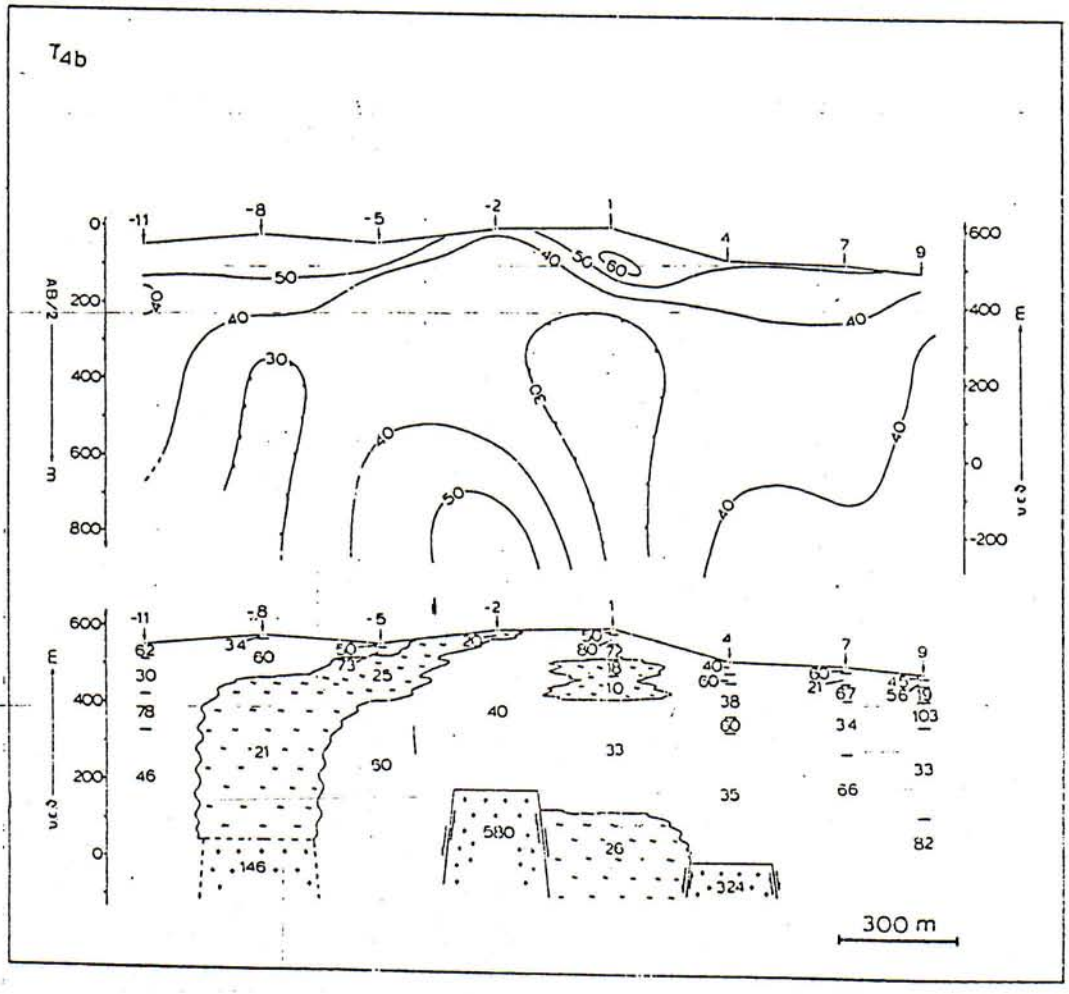

Fig. 5e

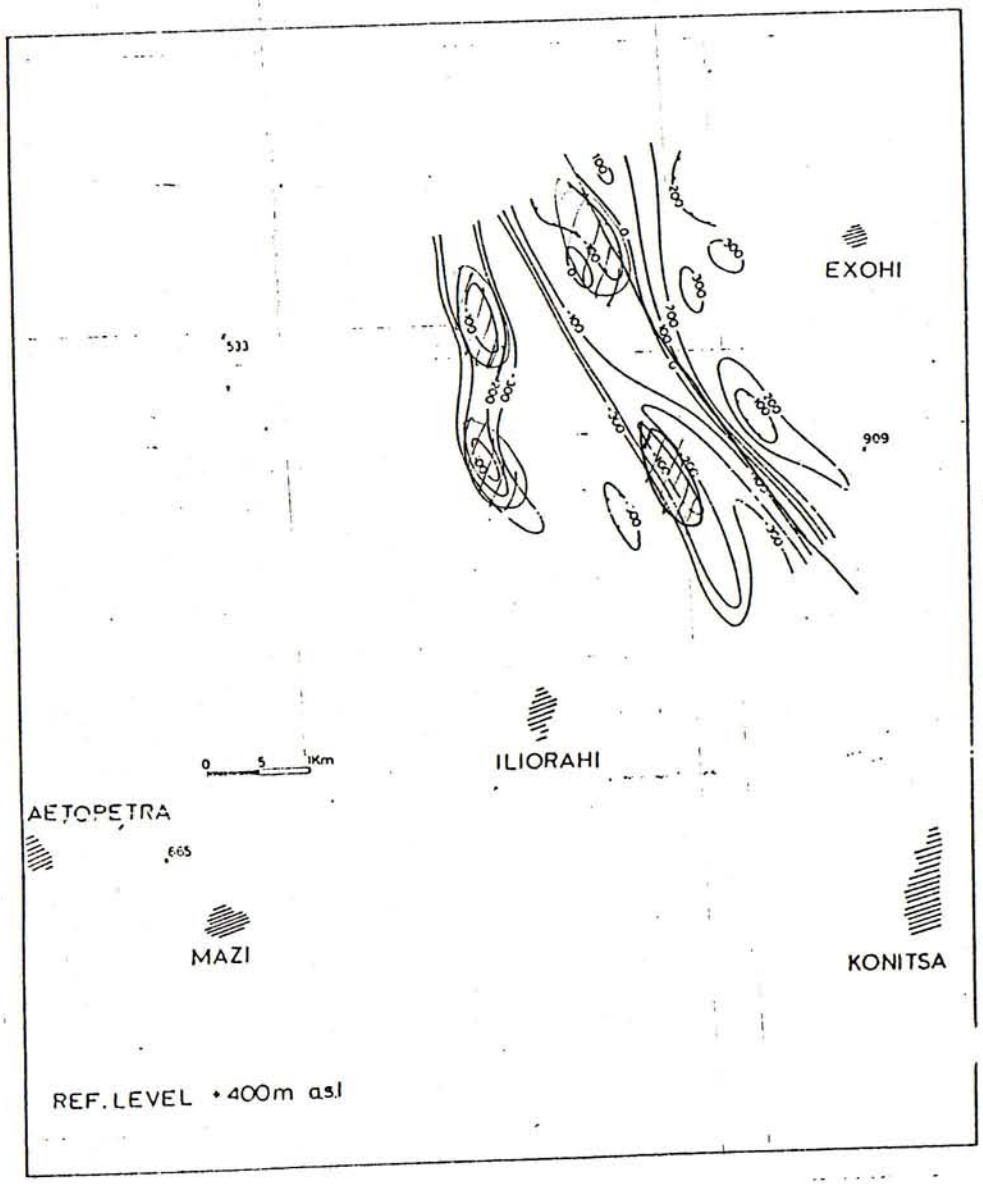
EXOHI
533
909
ILIORAHI
0 5 1Km
AETOPETRA
665
MAZI
KONITSA
REF. LEVEL +400m a.s.l

FIG. 7

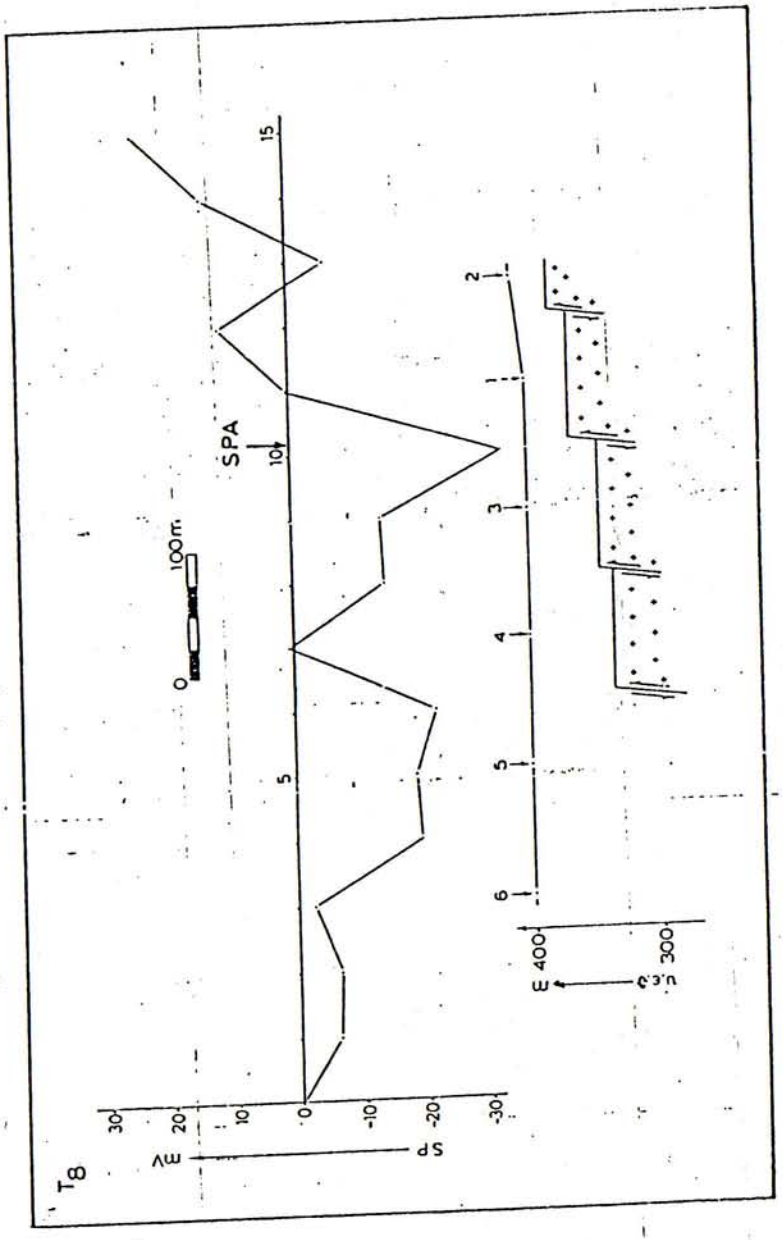
SPA
100m
0
15
10
5
2
3
4
5
6
E 400
300
mV
SP
30
20
10
0
-10
-20
-30
T8

FIG. 6a

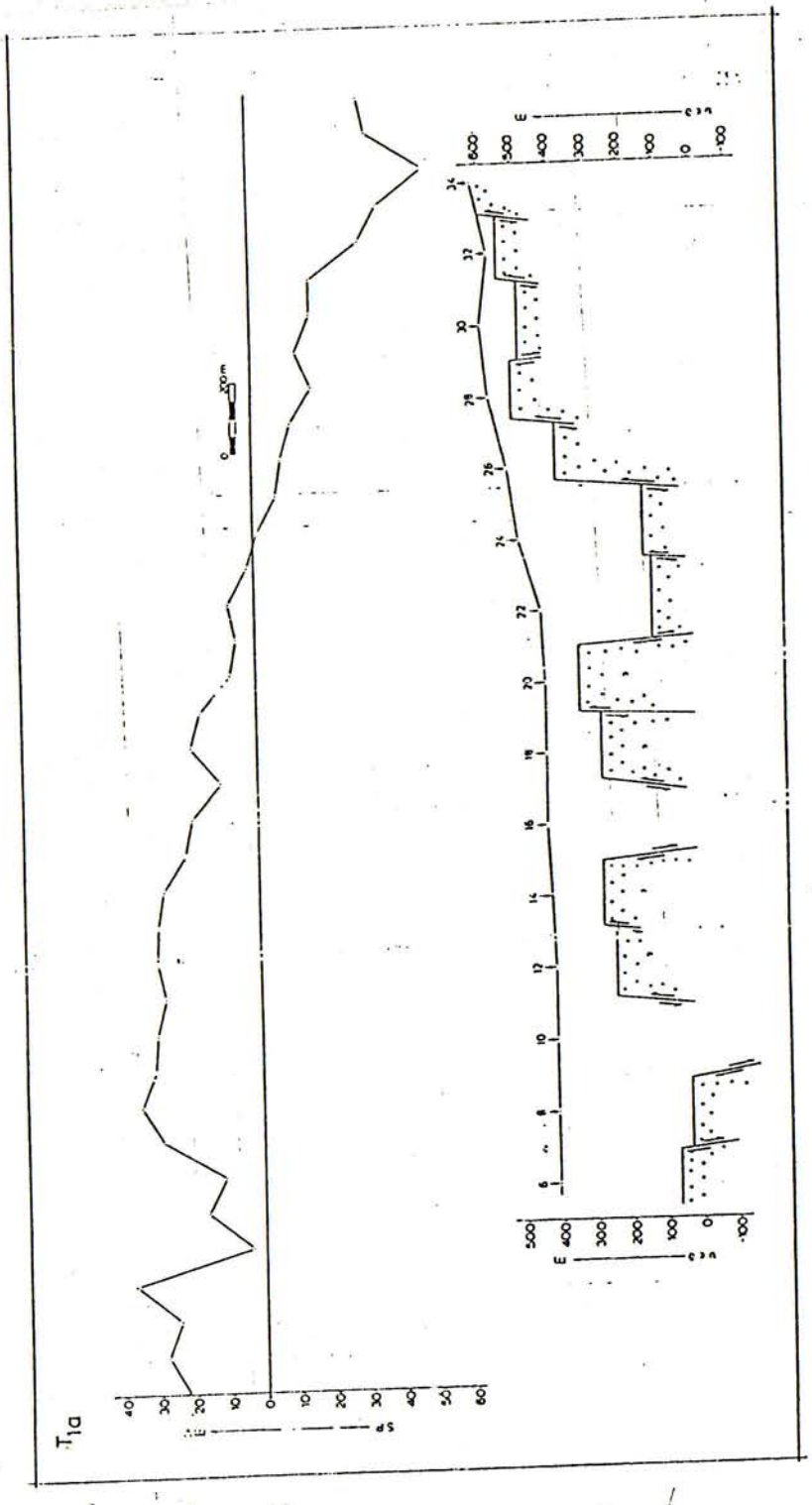
T1a
SP
E

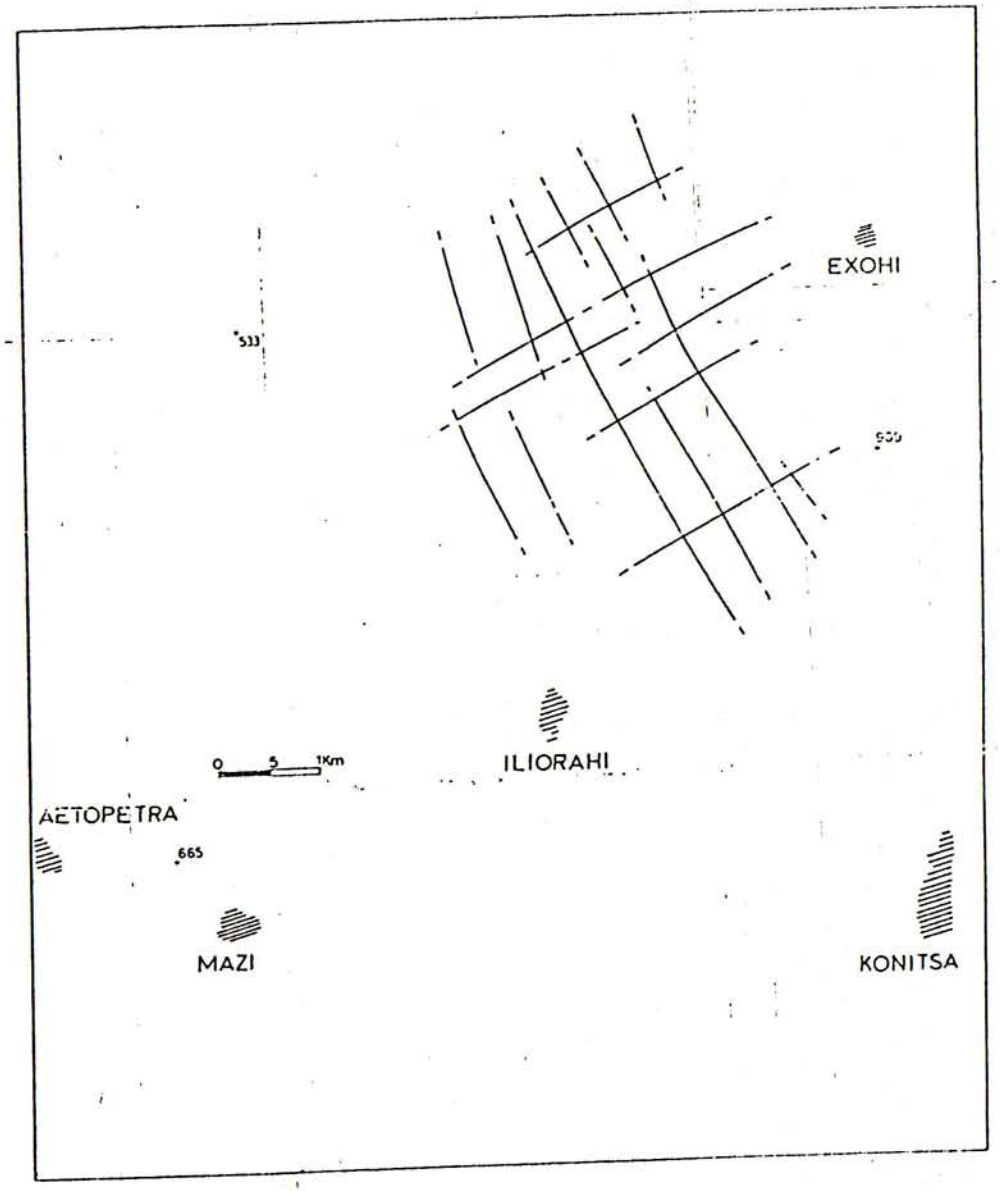
EXOHI
533
ILIORAHI
0 5 1Km
AETOPETRA
665
MAZI
KONITSA

FIG. 8

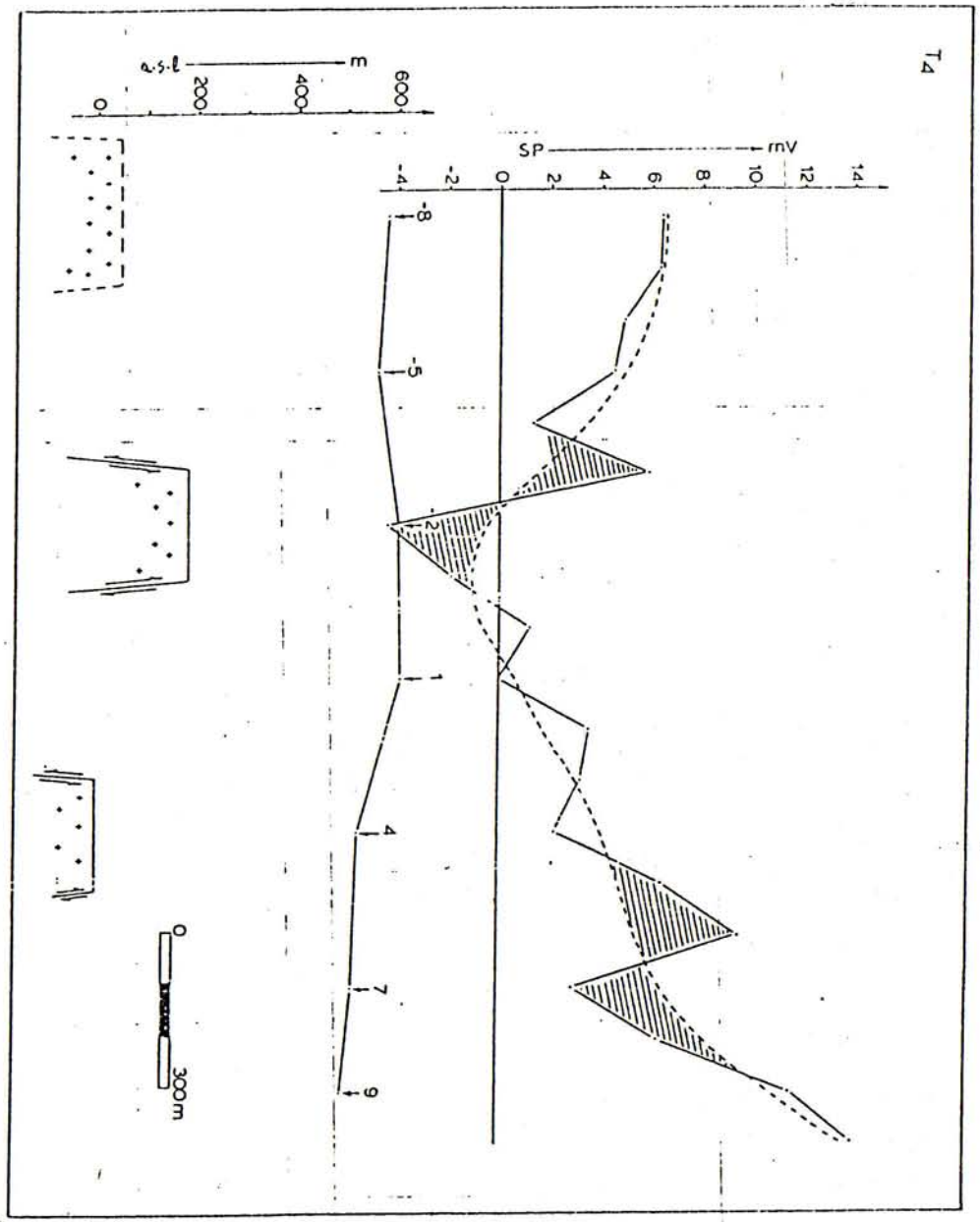
T4
E
p.s.e
0
200
400
600
SP
mV
-4
-2
0
2
4
6
8
10
12
14
-8
-5
-2
1
4
7
9
0
300m

FIG. 6d

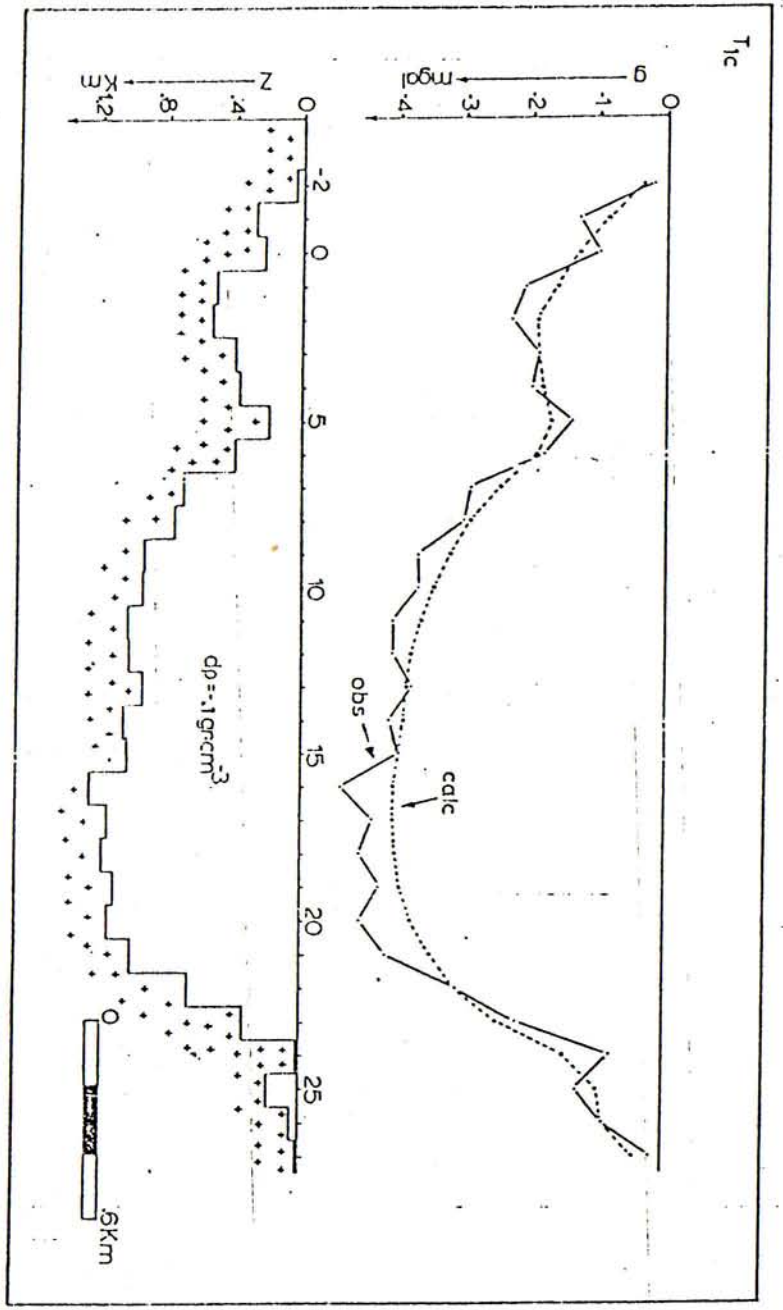
T1c
g
mgal
0
-1
-2
-3
-4
Z
X
E
0
.4
.8
1.2
-2
0
5
10
15
20
25
obs
calc
dρ=.1gr.cm⁻³
0
.5Km

FIG. 7

15 KM
20°30'
40°30'
40°00'
21°15'
-30
-20
-10
0
10
20
30
-23
-33
1
2
3
4
5
6

FIG. 10

BH-2
A
B
C
0
100
200
300
Core rec. %
T (C°)
W.L.
15
20
25
30

FIG. 11

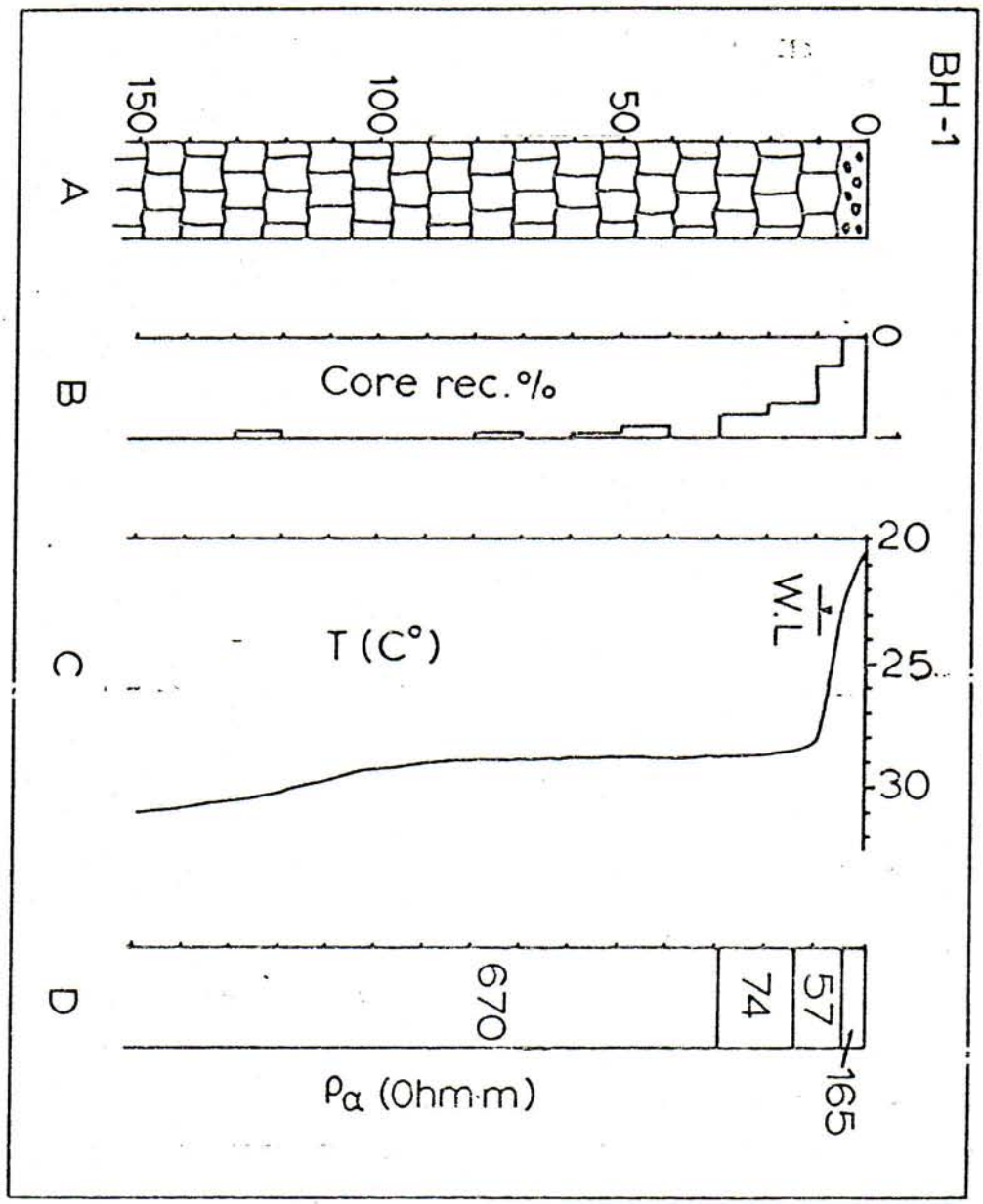
BH-1
150
100
50
0
A
B
Core rec.%
0
C
T (C°)
W.L
20
25
30
D
670
74
57
165
ρa (Ohm·m)

Fig. 4b

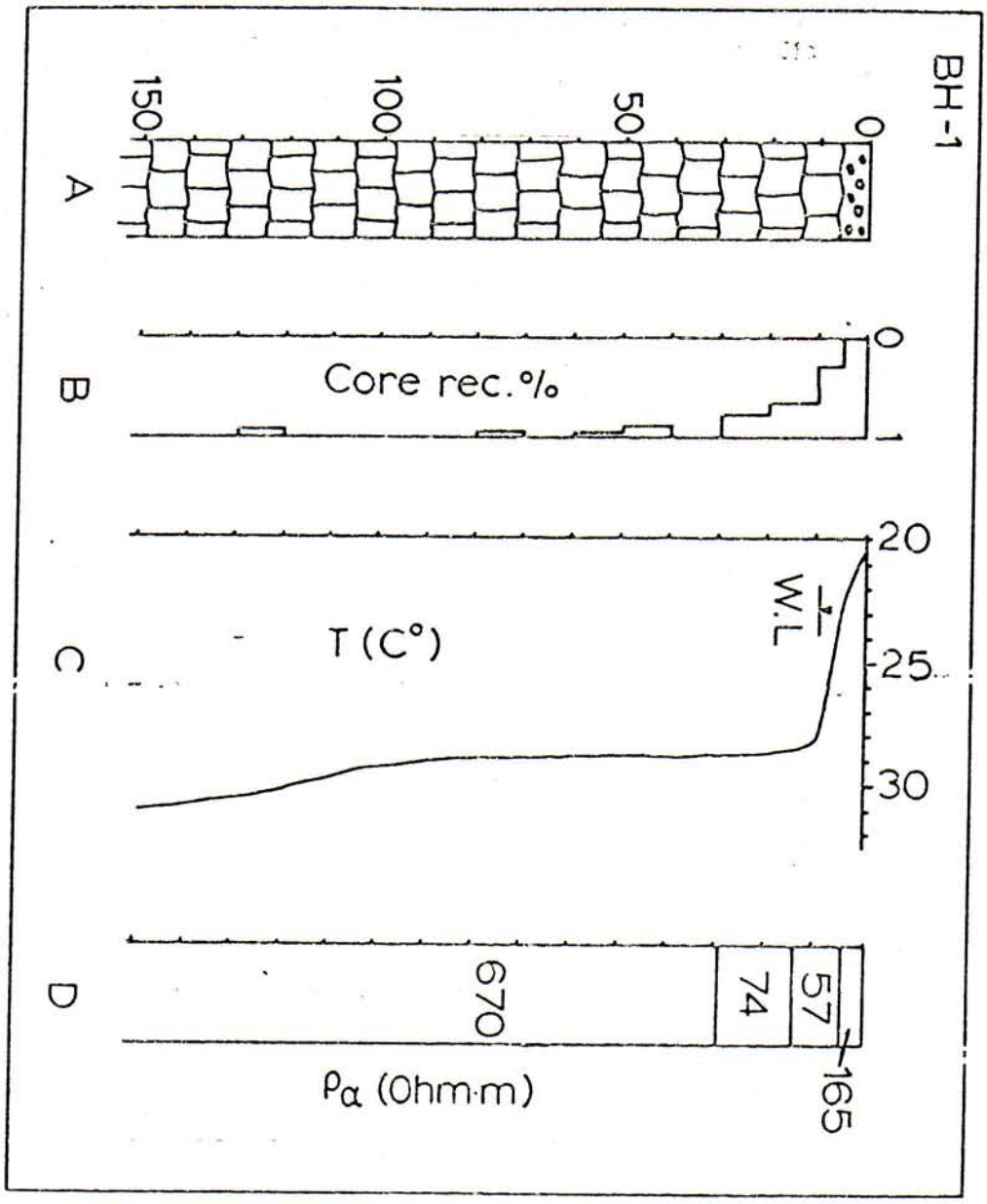
BH-1
150
100
50
0
A
B
Core rec.%
0
C
T (C°)
W.L
20
25
30
D
670
74
57
165
Pα (Ohm·m)

Fig. 4b